# PROCEEDINGS OF SPIE

SPIEDigitalLibrary.org/conference-proceedings-of-spie

Developing and evaluating the fidelity of patient specific kidney emulating phantoms for image-guided intervention applications

Kelly Merrell, Peter Jackson, Richard Simon, Cristian Linte

Kelly Merrell, Peter Jackson, Richard Simon, Cristian Linte, "Developing and evaluating the fidelity of patient specific kidney emulating phantoms for image-guided intervention applications," Proc. SPIE 12466, Medical Imaging 2023: Image-Guided Procedures, Robotic Interventions, and Modeling, 124661C (3 April 2023); doi: 10.1117/12.2655603



Event: SPIE Medical Imaging, 2023, San Diego, California, United States

# Developing and Evaluating the Fidelity of Patient Specific Kidney Emulating Phantoms for Image-guided Intervention Applications

Kelly Merrell<sup>a</sup>, Peter Jackson<sup>a</sup>, Richard Simon<sup>b</sup>, and Cristian Linte<sup>a,b</sup>

<sup>a</sup>Rochester Institute of Technology, Chester F. Carlson Center for Imaging Science, 54 Lomb Memorial Dr, Rochester, NY, 14623, USA

<sup>b</sup>Rochester Institute of Technology, Biomedical Engineering, 54 Lomb Memorial Dr, Rochester, NY, 14623, USA

#### ABSTRACT

Patient specific organ and tissue mimicking phantoms are used routinely to develop and assess new image-guided intervention tools and techniques in laboratory settings, enabling scientists to maintain acceptable anatomical relevance, while avoiding animal studies when the developed technology is still in its infancy. Gelatin phantoms, specifically, offer a cost-effective and readily available alternative to the traditional manufacturing of anatomical phantoms, and also provide the necessary versatility to mimic various stiffness properties specific to various organs or tissues. In this study, we describe the protocol to develop patient specific anthropomorphic gelatin kidney phantoms and we also assess the faithfulness of the developed phantoms against the patient specific CT images and corresponding virtual anatomical models used to generate the phantoms. We built the gelatin phantoms by first using additive manufacturing to generate a kidney mold based on patient specific CT images, into which the gelatin was poured. We then evaluated the fidelity of the phantoms (i.e., children) against the virtual kidney model generated from the patient specific CT image (i.e., parent) by comparing it to the surface model of the mold and gelatin phantoms (i.e., children) following their CT imaging post-manufacturing using various registration metrics. Our experiments showed a  $0.58 \pm 0.48$  mm surface-to-surface distance between the phantoms and mold models following landmark-based registration, and  $0.52 \pm 0.40$  mm surface-to-surface distance between the phantoms and the mold model following iterative closest point (ICP) registration. These experiments confirm that the described protocol provides a reliable, fast, and cost-effective method for manufacturing faithful patient specific organ emulating gelatin phantoms and can be applied or extended to other image-guided intervention applications.

**Keywords:** tissue mimicking gelatin phantoms, non-rigid anthropomorphic phantoms, patient specific organ geometry, image registration

#### 1. INTRODUCTION

Additive manufacturing has gained wide acceptance in the medical application domain and has provided alternative methods for producing anthropomorphic phantoms. These alternative methods are able to offer the phantom models the benefit of being customizable, readily accessible, and cost-effective. Fabrication of patient specific phantoms has aided many fields of research and clinical planning. The workflow to create 3D printed anatomic phantoms is often straight forward: start with segmenting the organ of interest from high resolution medical image dataset such as computed tomography (CT) or magnetic resonance (MRI), generate a surface model and subsequently a mesh model, which, for 3D printing applications is typically in the stereolithography (STL) format, then upload it into a computer aided design (CAD) software to print<sup>1,2</sup> the model.

Further author information: (Send correspondence to Kelly Merrell)

Kelly Merrell: E-mail: kam1217@rit.edu Peter Jackson: Email: pj7837@rit.edu Richard Simon: E-mail: rasbme@rit.edu Cristian Linte: Email: calbme@rit.edu

Medical Imaging 2023: Image-Guided Procedures, Robotic Interventions, and Modeling, edited by Cristian A. Linte, Jeffrey H. Siewerdsen, Proc. of SPIE Vol. 12466, 124661C © 2023 SPIE · 1605-7422 · doi: 10.1117/12.2655603

The above protocol enables the generation of mostly rigid phantoms, unless there exists access to special printing technologies and materials that enable the rapid prototyping of non-rigid models. Nevertheless, non-rigid organ emulating phantoms are in more need than the special 3D printers that are available, and hence versatile and cost-effective techniques to build such phantoms continue to be explored. The non-rigid material used in this study is a gelatin material. It was chosen because it is inexpensive, stable in nature, penetrable by needle, and fast to manufacture.

Similar work has shown that polyvinyl alcohol (PVA) cryogel is a popular material for the same reasons as gelatin. However, the manufacturing time for PVA extends over several days, and the PVA model must be stored in a water bath when not in use<sup>3,4</sup> to avoid dehydration and deterioration. Given its fewer constraints, gelatin is the favorable material to use to mimic soft tissue behavior. The opportunity to create tissue mimicking patient specific phantoms using gelatin could be achievable by most labs given have access to a 3D printer to generate a mold.

Maintaining the faithfulness of the manufactured gelatin phantoms relative to the original images is highly important. The work by Laing et al.<sup>4</sup> presented a method to assess the faithfulness of PVA- or silicon-based phantoms of the left atrium generated from patient-specific CT images by comparing the surface-to-surface distance of the registered atrium models. The open source software CloudCompare<sup>5</sup> provides features to calculate the distances between the virtual surface model generated from the CT image and and a surface model of the gelatin phantom generated from a CT image of the phantom post-manufacturing.

This study differs from the work by Laing et al.<sup>4</sup> as it provides several layers of evaluation of the fidelity of the phantom relative to the patient-specific CT image, the virtual model generated form the CT image and also the 3D printed mold used to manufacture the phantom. In addition, we also conduct a rudimentary study aimed at assessing the shelf-life of the phantoms and any changes in geometry over time. Hence, the motivation for this work is to develop a procedure workflow that can be utilized to assess the fidelity of a wide variety of tissue mimicking phantoms for lab-based research.

#### 2. METHODOLOGY

#### 2.1 Study Design Overview

Two kidney models (i.e., parent models) were created from an abdominal CT scan. Both models are of the same kidney, however, they differ by their surface fiducial configuration. The fiducials consisted of 1.5 mm radius hemispherical divots on the model surface. Each parent model featured 15 surface fiducials, six of which were later used as registration fiducials, and the remaining nine were used as target fiducials

The parent models were used to generate the 3D printed molds subsequently used to manufacture the gelatin phantoms. Three gelatin phantoms (i.e., children) were manufactured based on each of the two parent models and their corresponding molds. Following 3D printing of the molds and phantom manufacturing, CT images of both 3D printed molds and all six manufactured gelatin kidney phantoms were acquired.

Following image segmentation, surface models of the two parent molds and six children phantoms were generated and all surface fiducial landmarks were recorded. As later described, to assess the fidelity of the molds and the gelatin phantoms relative to the parent kidney models from the original CT images, the surface models of the two molds and six gelatin phantoms were registered back to their corresponding kidney models from the original CT images.

#### 2.2 Phantom Mold Design

The kidney phantoms were manufactured based on segmentation masks generated using the 3D Slicer open source software<sup>6</sup>. Following segmentation, a 3D model is rendered and exported from 3D Slicer as a Stand Tessellation Language (STL) file subsequently uploaded into Fusion  $360^7$  as a mesh and converted into a 3D body. The 3D mold was printed using a RostockMAX V3.2 3D printer using a 1.75 mm MatterHackers PRO Series PLA 3D printing filament, with the fill parameter set at 20% and layer parameter set at 0.2 mm. The mold was printed as two halves that can be assembled and disassembled to enable the extraction of the phantom, see Figure 1.



Figure 1. The 3D printed mold used to create the children phantoms. The mold was printed in two sections separated with respect to the sagittal plane allowing the gelatin phantom to be extracted.

### 2.3 Gelatin Preparation

The gelatin used for the phantoms in this study was the Humimic Medical Gelatin #0<sup>8</sup>. The phantom was built by melting cubes of the gelatin in a 400 mL beaker on a hot plate. The beaker was covered with aluminum foil, except when the gelatin needed to be stirred. The aluminum foil prevented any water from evaporating and decreased the melting time. Once the gelatin turned into a liquid consistency, it was poured into the bottom half of the mold in layered increments. Since gelatin cools rapidly, once the consistency of the gelatin changed, the beaker was re-heated on the hot plate and the melting and pouring process was repeated. After the bottom half of the mold was filled, it was connected to the top half of the mold and fixed together with a bar clamp. To help ensure the gelatin is completely filling the mold, the mold was slightly rotated while pouring, while the fill hole was cleaned in between pours to prevent clogging. The gelatin phantom was removed from the mold three hours after the final pour and it was ready to be used. Note that the 3-hour settling time was based on a volume of the kidney mold of 174 mL, so larger molds will need additional time to fully cure.

#### 2.4 Phantom Imaging

All manufactured phantoms and 3D printed molds were imaged using a PiXS CT PXS - 255/60 CT imaging system by Pinnacle X-Ray Solutions using the following scanning parameters: 100 kV, 400 mA, 720 projections over 360 degrees of rotation, and  $2 \times 2 \text{ binning}$ . The reconstruction of the raw data from the CT scan was done with Volume Graphics VGSTUDIO MAX software.

#### 2.5 Fiducial Location

All CT images were imported into 3D Slicer and a surface model was rendered and used to identify the coordinates of all fifteen surface fiducial landmarks (i.e., hemispherical divots) using the axial, sagittal and coronal imaging planes. Each of the 15 fiducial landmarks was localized 10 times, with the ground truth location of each fiducial characterized as the centroid of the 10 successive localizations. This exercise enabled us to assess the localization error (FLE) associated with each of the 15 fiducials, as well as the overall FLE computed across all 15 fiducial landmarks, each samples 10 times, computed as the RMS FLE.

# 2.6 Mold and Phantom Fidelity Assessment

A two-step registration approach was employed to compare the manufactured gelatin phantoms to the molds used to build them and also to the organ geometry depicted in the original CT images. We first performed a landmark-based registration, where the six registration fiducials were employed, then assessed the registration according to the FRE (across the six registration fiducials), TRE (across the remaining nine target fiducials not employed for registration), and surface TRE (surface-to-surface distance post-registration). We then also

performed a surface-based registration refinement using the iterative closest point (ICP) algorithm<sup>4,5</sup>, which we also assessed according to the TRE (evaluated across the nine target fiducials) and surface TRE (surface-to-surface distance post-registration).

#### 2.7 Gelatin Shelf Life

The shelf life of the gelatin was evaluated by repeating the CT images of the same phantom two months apart, initial and final, and compare their surface TRE. The surface TRE of the initial phantom to the mold, and the final phantom and the mold will also be evaluated. The closest registration possible was needed to assess the stability of the material. This was accomplish by first using all 15 of the surface fiducials to perform a landmark registration. After the landmark registration, an ICP registration was performed to further ensure the closest registration.

#### 3. RESULTS

### 3.1 Fiducial Localization Error (FLE) Evaluation

Since the fiducials and their localization plays a crucial role in the evaluation, we first assessed the FLE. The FLE associated with each of the 15 fiducial landmarks ranged from 0.18 mm to 0.30 mm, with an overall average of 0.24 mm.

## 3.2 Phantom and Mold Fidelity Assessment via Registration

To assess the fidelity of the mold and phantoms relative to the original parent CT images, we registered the surface models of the kidney extracted from the molds' CT images and all manufactured phantoms' CT images to the surface model of the kidney extracted from the original patient specific CT images. A first registration was performed using landmark-based registration, which was evaluated in terms of the FRE, TRE and surface TRE, then refined using ICP registration, also evaluated in terms of TRE and surface TRE.

Table 1 shows the registration statistics between the mold and phantoms relative to the parent kidney models. The results are consistent across both sets of kidney geometries (1) and (2). Moreover, both landmark-based registration and ICP registration led to RMS TRE under 1 mm, but the ICP refinement appears to have further slightly improved the overall surface-to-surface distance (surface TRE) beyond that achieved using landmark-based registration. Overall, these results suggest that both the 3D printed molds and fabricated phantoms are within less than 1 mm of the kidney geometry depicted in the patient specific CT images.

Table 1. Summary of the comparison between the mold models and phantom models relative to the parent kidney models from original CT images. The surface models of the molds and gelatin phantoms extracted from CT images post-manufacturing were registered to the surface models of the kidney extracted from the original CT images. A landmark-based registration was first performed using 6 of the 15 landmarks and assessed using the RMS FRE, TRE and surface TRE (left columns), then refined using an ICP registration assessed using the RMS TRE and surface TRE (right columns).

Registration	Landmark-based Registion Error (RMS)			ICP-based Registration Error (RMS)	
Model	FRE (mm)	TRE (mm)	Surface TRE (mm)	TRE (mm)	Surface TRE (mm)
Parent 1 Model	S1	_	=	<u> </u>	-
Parent 1 Mold	0.76	0.96	0.47	1.00	0.43
Child 1A Phantom	0.54	0.75	0.82	1.22	0.62
Child 1B Phantom	0.57	0.65	0.77	1.20	0.57
Child 1C Phantom	0.86	1.10	1.15	1.39	0.95
Parent 2 Model			9	9	7-
Parent 2 Mold	0.95	0.92	0.46	1.54	0.44
Child 2A Phantom	0.39	0.79	0.59	1.18	0.48
Child 2B Phantom	0.53	0.86	0.84	1.03	0.72
Child 2C Phantom	0.63	0.87	0.68	1.18	0.60

Similarly, Table 2 reports a similar comparison, however relative to the mold models, rather than the original kidney models from the CT images. Once again, the landmark-based registration, although acceptable given a

less than 1 mm RMS TRE, was further slightly improved following ICP refinement. Lastly, the kidney geometry was sufficiently well preserved between the original CT image, 3D printing of the mold, and gelatin phantom manufacturing, as supported by the less than 1 mm overall RMS surface TRE.

Table 2. Summary of the comparison between the mold models and phantom models relative to the parent kidney models from original CT images. The surface models of the molds and gelatin phantoms extracted from CT images post-manufacturing were registered to the surface models of the kidney extracted from the original CT images. A landmark-based registration was first performed using 6 of the 15 landmarks and assessed using the RMS FRE, TRE and surface TRE (left columns), then refined using an ICP registration assessed using the RMS TRE and surface TRE (right columns).

Registration	Landmark-based Registion Error (RMS)			ICP-based Registration Error (RMS)	
Model	FRE (mm)	TRE (mm)	Surface TRE (mm)	TRE (mm)	Surface TRE (mm)
Parent 1 Model	0.76	0.96	0.49	2.10	0.43
Parent 1 Mold	( <u>188</u> )	2	120	2	72
Child 1A Phantom	0.71	0.72	0.82	1.00	0.71
Child 1B Phantom	0.80	0.77	0.78	1.15	0.68
Child 1C Phantom	1.08	1.06	1.15	2.05	1.00
Parent 2 Model	0.95	0.92	0.48	1.38	0.46
Parent 2 Mold	-	-	120	¥1	84
Child 2A Phantom	0.90	0.84	0.70	2.77	0.58
Child 2B Phantom	0.97	0.89	1.08	2.78	0.98
Child 2C Phantom	1.01	0.93	0.90	2.15	0.82

Figure 2 presents a graphical, visual comparison of the overall effect of using landmark-based registration vs. a ICP registration between a phantom model and its corresponding mold model. As shows, the landmark-based registration provides similar alignment as the ICP registration, with the exception that the latter leads to an ever so slightly more accurate overall alignment, as also supported by the surface TRE following landmark-based vs. ICP registration reported in Table 1 and Table 2. Note that the maximum distance error is the result of an air bubble that formed while setting up in the mold. The location of the air bubble is present in Figure 2 as the red area on the surface.

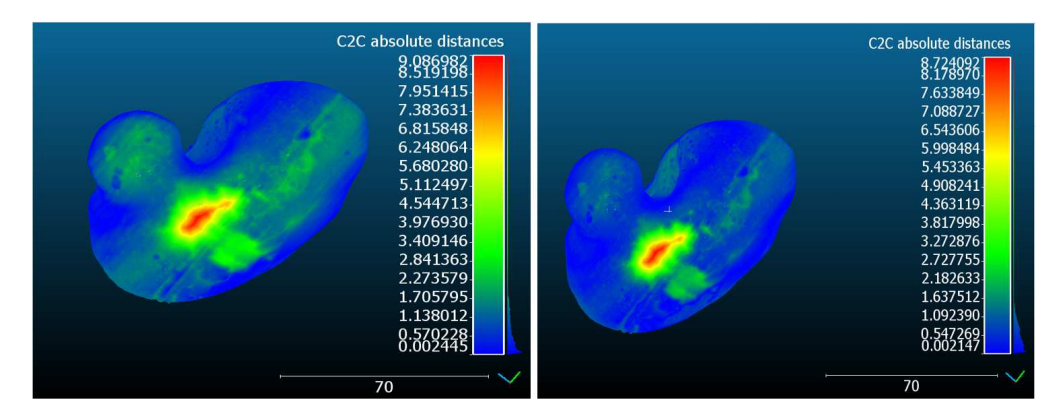


Figure 2. Effect of the landmark vs. ICP registration between a phantom model and its corresponding mold model. Note the overall improved surface-to-surface distance (i.e., surface TRE) achieved following ICP registration.

# 3.3 Gelatin Shelf Life Assessment

The stability of the gelatin material is important to evaluate. If the material were to change size dimensions over time that would have a negative affect on the outcome of the experiment. The gelatin Child 1B Phantom had CT images obtained within a week of manufacturing and had CT images obtained again after a time period of two months. During the two month time period, the gelatin phantom was stored in open air where is was exposed to light from windows and typical overhead laboratory lighting. The registration FRE calculated from

using the 15 fiducials is 0.33 mm. The surface TRE from the landmark registration is 0.34 mm and the ICP registration process determined a surface TRE of 0.33 mm. The FRE of the landmark based registration of the initial to mold and the final to mold are respectfully 1.05 mm and 0.99 mm, the surface TRE before ICP 0.92 mm and 1.12 mm, and finally the ICP surface TRE is 0.82 mm and 0.97 mm.

#### 4. DISCUSSION, CONCLUSION AND FUTURE WORK

We have presented an accurate method to produce tissue mimicking patient specific phantoms from a gelatin material. The experiment shows that this developed method can produce phantoms that are within  $0.52\pm0.40$  mm from the geometry depicted in the pre-operative CT images. The gelatin phantoms are stable within 0.33 mm between CT images obtained two months apart, and can retail their shape until melted again<sup>8</sup>. This method will be further applied to building gelatin liver phantoms that will be used for non-rigid deformable registration studies. This paper will serve as a reference for researchers in need of creating custom anatomical tissue mimicking phantoms.

This work described the full protocol associated with the design and manufacture of patient specific molds and gelatin phantoms for image-guided renal interventions applications, along with a detailed protocol designed to assess the faithfulness of the 3D printed molds and subsequently, manufactured phantoms relative to the original patient specific kidney models generated from the original images. This study demonstrates a versatile workflow for generating non-rigid patient specific organ and tissue emulating phantoms in a rapid and cost-effective fashion in any reasonably equipped laboratory.

#### 5. ACKNOWLEDGEMENT

Research reported in this publication was supported by the National Institute of General Medical Sciences of the National Institutes of Health under Award No. R35GM128877 and by the Office of Advanced Cyber-infrastructure of the National Science Foundation under Award No. 1808530.

### REFERENCES

- [1] Abdullah, K. A. and Reed, W., "3D printing in medical imaging and healthcare services," *Journal of medical radiation sciences* **65**(3), 237–239 (2018).
- [2] Craft, D. F. and Howell, R. M., "Preparation and fabrication of a full-scale, sagittal-sliced, 3d-printed, patient-specific radiotherapy phantom," *Journal of applied clinical medical physics* **18**(5), 285–292 (2017).
- [3] Surry, K. J. M., Austin, H. J. B., Fenster, A., and Peters, T. M., "Poly(vinyl alcohol) cryogel phantoms for use in ultrasound and MR imaging," *Physics in Medicine and Biology* **49**, 5529–5546 (dec 2004).
- [4] Laing, J., Moore, J., Bainbridge, D., Drangova, M., and Peters, T., "Patient-specific atrium models for training and pre-procedure surgical planning," in [Medical Imaging 2017: Image-Guided Procedures, Robotic Interventions, and Modeling], III, R. J. W. and Fei, B., eds., 10135, 330 – 337, International Society for Optics and Photonics, SPIE (2017).
- [5] https://www.danielgm.net/cc/.
- [6] https://www.slicer.org/.
- $[7] \ https://www.autodesk.com/products/fusion-360/overview?term=1-YEARtab=subscription.$
- [8] https://humimic.com/product/gelatin-0-ballistic-gelatin-by-the-pound/.